Efficient interfacing photonic and long-range dielectric-loaded plasmonic waveguides

Yiting Chen,[1] Vladimir A. Zenin,[1] Kristjan Leosson,[2] Xueliang Shi,[3] Michael G. Nielsen,[1] and Sergey I. Bozhevolnyi[1]*

[1]*Centre for Nano Optics, University of Southern Denmark, Niels Bohrs Allé 1, DK-5230 Odense M, Denmark*

[2]*Innovation Center Iceland, Arleynir 2-8, IS112 Reykjavik, Iceland and Science Institute, University of Iceland, Dunhagi 3, IS107 Reykjavik, Iceland*

[3]*Department of Information Science and Electronic Engineering, Zhejiang University, Hangzhou 310027, China*

*seib@iti.sdu.dk

Abstract: Long-range dielectric-loaded surface plasmon-polariton waveguides (LR-DLSPPWs) operating at telecom wavelengths are efficiently (end-fire) interfaced with photonic waveguides by taking advantage of very similar lateral mode field profiles in these waveguide configurations. The LR-DLSPPWs are formed by 1-μm-high and 1-μm-wide polymer ridges fabricated atop 15-nm-thin and 500-nm-wide gold stripes supported by a 289-nm-thick ormoclear polymer deposited on a low-index (1.34) layer of cytop, whereas gold stripes are absent in the photonic waveguide configuration that is identical to the plasmonic one in all other respects. The coupling efficiency between LR-DLSPPWs and photonic waveguides is numerically estimated to be 97%, decreasing by only a few percents for non-centered gold stripes (as long as a gold stripe is kept inside the polymer ridge). The fabricated LR-DLSPPWs coupled to photonic waveguides are first characterized using amplitude- and phase-resolved near-field imaging of propagating radiation that reveals very similar mode field distributions in these waveguides as well as their efficient interfacing. The coupling efficiency is then experimentally characterized using the cutback approach resulting in an average level of 75% per interface, while the LR-DLSPPW mode propagation length is estimated to be on average 0.3 mm. Possible reasons for differences between experimental and simulation results are discussed, indicating that a 3-nm-thin titanium layer (used for improving adhesion between gold and ormoclear) introduces substantial mode absorption. The results obtained open new perspectives for realization of hybrid photonic-plasmonic components and circuits.

OCIS codes: (230.7370) Waveguides; (240.6680) Surface plasmons; (250.5403) Plasmonics.

References and links

1. W. L. Barnes, A. Dereux, and T. W. Ebbesen, "Surface plasmon subwavelength optics," Nature **424**, 824–830 (2003).

#233873 - $15.00 USD Received 5 Feb 2015; revised 24 Mar 2015; accepted 24 Mar 2015; published 1 Apr 2015

2. D. K. Gramotnev and S. I. Bozhevolnyi, "Plasmonics beyond the diffraction limit," Nat. Photonics **4**, 83–91 (2010).
3. E. Ozbay, "Plasmonics: merging photonics and electronics at nanoscale dimensions," Science **311**, 189–193 (2006).
4. R. M. Briggs, J. Grandidier, S. P. Burgos, E. Feigenbaum, and H. A. Atwater, "Efficient coupling between dielectric-loaded plasmonic and silicon photonic waveguides," Nano Lett. **10**, 4851-4857 (2010).
5. M. Hochberg, T. Baehr-Jones, C. Walker, and A. Scherer, "Integrated plasmon and dielectric waveguides," Opt. Express **12**, 5481–5486 (2004).
6. O. Tsilipakos, A. Pitilakis, T. V. Yioultsis, S. Papaioannou, K. Vyrsokinos, D. Kalavrouziotis, G. Giannoulis, D. Apostolopoulos, H. Avramopoulos, T. Tekin, M. Baus, M. Karl, K. Hassan, J. Weeber, L. Markey, A. Dereux, A. Kumar, S. I. Bozhevolnyi, N. Pleros, and E. E. Kriezis, "Interfacing dielectric-loaded plasmonic and silicon photonic waveguides: theoretical analysis and experimental demonstration," IEEE J. Quantum Electron. **48**, 678–687 (2012).
7. L. Liu, Z. Han, and S. He, "Novel surface plasmon waveguide for high integration," Opt. Express **13**, 6645–6650 (2005).
8. D. F. P. Pile, T. Ogawa, D. K. Gramotnev, Y. Matsuzaki, K. C. Vernon, K. Yamaguchi, T. Okamoto, M. Haraguchi, and M. Fukui, "Two-dimensionally localized modes of a nanoscale gap plasmon waveguide," Appl. Phys. Lett. **87**, 261114 (2005).
9. S. I. Bozhevolnyi, V. S. Volkov, E. Devaux, J. Y. Laluet, and T. W. Ebbesen, "Channel plasmon subwavelength waveguide components including interferometers and ring resonators," Nature **440**, 508–511 (2006).
10. M. Yan and M. Qiu, "Guided plasmon polariton at 2D metal corners," J. Opt. Soc. Am. B **24**, 2333–2342 (2007).
11. X. Guo, M. Qiu, J. Bao, B. J. Wiley, Q. Yang, X. Zhang, Y. Ma, H. Yu, and L. Tong, "Direct coupling of plasmonic and photonic nanowires for hybrid nanophotonic components and circuits," Nano Lett. **9**, 4515-4519 (2009).
12. W. Wang, Q. Yang, F. Fan, H. Xu, and Z. Wang, "Light propagation in curved silver nanowire plasmonic waveguides," Nano Lett. **11**, 1603–1608 (2011).
13. S. I. Bozhevolnyi, A. Boltasseva, T. Søndergaard, T. Nikolajsen, and K. Leosson, "Photonic bandgap structures for long-range surface plasmon polaritons," Opt. Commun. **250**, 328–333 (2005).
14. P. Berini, R. Charbonneau, N. Lahoud, and G. Mattiussi, "Characterization of long-range surface-plasmon-polariton waveguides," J. Appl. Phys. **98**, 043109 (2005).
15. T. Holmgaard, J. Gosciniak, and S. I. Bozhevolnyi, "Long-range dielectric-loaded surface plasmon-polariton waveguides," Opt. Express **18**, 23009–23015 (2010).
16. X. Shi, X. Zhang, Z. Han, U. Levy, and S. I. Bozhevolnyi, "CMOS-compatible long-range dielectric-loaded plasmonic waveguides," J. Lightwave Technol. **31**, 3361-3367 (2013).
17. J. Gosciniak, S. I. Bozhevolnyi, T. B. Andersen, V. S. Volkov, J. Kjelstrup-Hansen, L. Markey, and A. Dereux, "Thermo-optic control of dielectric-loaded plasmonic waveguide components," Opt. Express **18**, 1207–1216 (2010).
18. J. Gosciniak, L. Markey, A. Dereux, and S. I. Bozhevolnyi, "Efficient thermo-optically controlled Mach-Zhender interferometers using dielectric-loaded plasmonic waveguides," Opt. Express **20**, 16300-16309 (2012).
19. J. Gosciniak and S. I. Bozhevolnyi, "Performance of thermo-optic components based on dielectric-loaded surface plasmon polariton waveguides," Sci. Rep. **3**, 1803 (2013).
20. V. S. Volkov, Z. Han, M. G. Nielsen, K. Leosson, H. Keshmiri, J. Gosciniak, O. Albrektsen, and S. I. Bozhevolnyi, "Long-range dielectric-loaded surface plasmon polariton waveguides operating at telecommunication wavelengths," Opt. Lett. **36**, 4278-4280 (2011).
21. V. A. Zenin, Z. Han, V. S. Volkov, K. Leosson, I. P. Radko, and S. I. Bozhevolnyi, "Directional coupling in long-range dielectric-loaded plasmonic waveguides," Opt. Express **21**, 8799-8807 (2013).
22. R. Zektzer, B. Desiatov, N. Mazurski, S. I. Bozhevolnyi, and U. Levy, "Experimental demonstration of CMOS-compatible long-range dielectric-loaded surface plasmon-polariton waveguides (LR-DLSPPWs)," Opt. Express **22**, 22009-22017 (2014).
23. T. Holmgaard and S. I. Bozhevolnyi, "Theoretical analysis of dielectric-loaded surface plasmon-polariton waveguides," Phys. Rev. B **75**, 245405 (2007).
24. G. I. Kweon and I. S. Park, "Splicing losses between dissimilar optical waveguides," J. Lightw. Technol. **17**, 690-703 (1999).
25. P. Johnson and R. Christy, "Optical constants of the noble metals," Phys. Rev. B **6**(12), 4370–4379 (1972).
26. M. Palamaru and P. Lalanne, "Photonic crystal waveguides: out-of-plane losses and adiabatic modal conversion," Appl. Phys. Lett. **78**, 1466–1468 (2001).
27. A. Andryieuski, V. A. Zenin, R. Malureanu, V. S. Volkov, S. I. Bozhevolnyi, and A. V. Lavrinenko, "Direct characterization of plasmonic slot waveguides and nanocouplers," Nano Lett. **14**, 3925-3929 (2014).
28. N. Ocelic, A. Huber, and R. Hillenbrand, "Pseudoheterodyne detection for background-free near-field spectroscopy," Appl. Phys. Lett. **89**, 101124 (2006).
29. A. Garcia-Etxarri, I. Romero, F. J. Garcia de Abajo, R. Hillenbrand, and J. Aizpurua, "Influence of the tip in near-field imaging of nanoparticle plasmonic modes: weak and strong coupling regimes," Phys. Rev. B **79**, 125439 (2009).

#233873 - $15.00 USD Received 5 Feb 2015; revised 24 Mar 2015; accepted 24 Mar 2015; published 1 Apr 2015

1. Introduction

Surface plasmon polaritons (SPPs) is a hybrid wave of light and collective free electron oscillations in a dielectric and metallic interface, with the extraordinary ability of manipulating and routing light at the nanoscale, as well as strong field enhancement [1]. Scientists have been expecting the realization of plasmonic circuit, which would have the compactness of an electronic circuit and broad bandwidth of photonic network [2, 3]. However, due to the large propagation loss from the metallic composition, it has been a big challenge to realize plasmonic circuits. An alternative is hybrid photonic-plasmonic circuit [4–6], which employs plasmonic components only where high efficiency, low power consumption (for active components) and (or) small footprint is required, and leaves low-loss photonic waveguides to interconnect such components. In this case, efficient interconnection between plasmonic and photonic waveguides will be very important and necessary. In this paper, we present photonic-plasmonic waveguides that are seamlessly interfaced with high coupling efficiency.

In past decades, many different types of plasmonic waveguides have been proposed and realized, such as slot waveguides [7, 8], channel or wedge waveguides [9, 10], metallic nanowires [11, 12] etc. These plasmonic waveguides exhibt strong sub-wavelength field confinement (even as small as in nanometer scale), but suffer from large propagation loss. Meanwhile, long-range SPP waveguides (LRSPPWs) [13, 14], with a thin gold film embedded between two dieletric layers, show the potential of long propagation length (in centimeter order), but in the cost of weak field confinement. Different from those two extreme situations, LR-DLSPPWs [15, 16], with a gold stripe sandwiched between a dielectric ridge and film (Fig. 1(a)), show good balance between propagation loss and field confinement, with millimeter-long propagation lengths and wavelength-sized mode confinement, which makes it a good candidate to integrate with photonic waveguides. Besides, the embedded gold stripe could also transmit electrical signals, which might be used to control the appropriately designed component through thermo-optic or electric-optic effects [17–19]. Due to these advantages, LR-DLSPPWs have attracted considerable attention, with several experimental realizations being reported in recent years [20–22]. Here, we design and experimentally demonstrate high-efficiency coupling between photonic waveguides and LR-DLSPPWs that are seamlessly interfaced, with the only difference being the presence of a gold stripe at the core of LR-DLSPPWs. This demonstration shows the potential of efficient integration of LR-DLSPPWs into photonic circuits. Our choice of gold for the LR-DLSPPW configuration is motivated by the circumstance that, at telecom wavelengths, gold and silver (usually used plasmonic metals) have similar properties, while gold is chemically more stable than silver. In this paper, we first present the design and simulations of the LR-DLSPPW configuration as well as its interfacing with photonic waveguides. Then, the experimental characterization of LR-DLSPPW and photonic mode properties and their coupling loss is reported and discussed.

2. Waveguide configuration and simulation

The considered LR-DLSPPW configuration includes a dielectric ridge deposited on a metal stripe supported by a layered dielectric structure, with a sufficiently thick bottom film having a low refractive index [Fig. 1(a)] in order to prevent the mode from leaking downwards into a silicon substrate, ensuring thereby good mode confinement. We fabricated the LR-DLSPPWs first by spin-coating 4.3-μm-thick cytop and 289-nm-thick ormoclear films onto a silicon wafer. Then 500-nm-wide gold stripes are patterned by electron beam lithography (EBL), thermal evaporation of a 15-nm-thin gold film (on a 3-nm-thin titanium film to increase the adhesion between gold and ormoclear) and lift-off. The final step of fabrication is the patterning of the PMMA ridge by means of second exposure of EBL. The width and height of the ridge are both 1 μm. From top to bottom, refractive indexes of PMMA, ormoclear and cytop (at 1550

#233873 - $15.00 USD Received 5 Feb 2015; revised 24 Mar 2015; accepted 24 Mar 2015; published 1 Apr 2015

nm) are 1.493, 1.535 and 1.34, respectively [Fig. 1(a)]. Figure 1(b) presents the distribution of dominating electric field component $|\mathbf{E}_y|$ of the fundamental transverse magnetic (TM) mode at 1550 nm in LR-DLSPPW, with the effective mode index ($\mathbf{N}_{eff}$) of 1.363, while Fig. 1(c) shows that of fundamental TM mode in photonic waveguide which has the exact same configuration as the LR-DLSPPW except without the gold stripe, with the $\mathbf{N}_{eff}$ of 1.357. From those two field distribution figures, we can see that both TM modes have very similar mode profile, which promises high coupling efficiency between them.

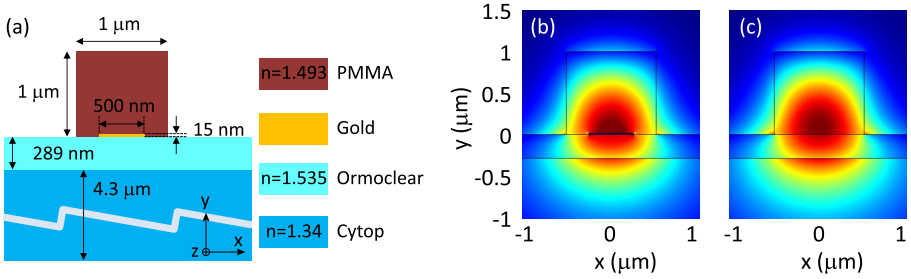

Fig. 1. (a) Schematic cross section of a straight LR-DLSPPW with a PMMA ridge atop a gold stripe supported by ormoclear and cytop films deposited on a silicon wafer. Field distributions of dominating electric field component $|\mathbf{E}_y|$ in fundamental mode $\mathbf{TM}_{00}$ at 1550 nm (b) in the LR-DLSPPW and (c) in the photonic waveguide (which has the exact same configuration as in (b) except without the gold stripe).

There has been comprehensive theoretical analysis on LR-DLSPPWs [15, 16, 23]. In those papers, influences of geometric parameters of waveguide, such as buffer layer thickness, ridge size, gold stripe dimension on the field confinement, propagation length ($\mathbf{L}_p$) have been carefully investigated, thus offering a good guide to optimize the design of LR-DLSPPWs. However, in the process of fabrication, deviation of several parameters, such as gold stripe displacement, and gold stripe thickness ($\mathbf{t}_{Au}$), may play an important role in the performance of the waveguides. Besides, the introduction of titanium layer, which is very commonly used in the deposition of gold film to increase the adhesion between gold film and the dielectric material, can also exert remarkable influence on the performance of the waveguides. Therefore, we carried out some simulation by means of commercial software COMSOL MULTIPHYSICS, to study the impact of the above parameters. The dispersive permittivities of gold and titanium are obtained from the data measured by Johnson and Christy [25]. The results are shown in Fig. 2. Figure 2(a) shows the dependence of propagation length on the gold stripe displacement with different thicknesses. Without the displacement of gold stripe, LR-DLSPP mode has largest propagation length for gold stripe thickness of around 10 nm. It is noticed that even when the gold stripe is displaced by 100 nm, the propagation length only decreases about 10%. This shows good fabrication tolerance to the placement of the gold stripe. However, the propagation length is very sensitive to the thickness of the gold stripe. When the thickness increases from 10 nm to 20 nm, the propagation length decreases from 6 mm to 1.8 mm, due to the increasing loss in the gold stripe. However, due to practical consideration related to fabrication and interfacing to external electrode, we choose the thickness of 15 nm [15].

The coupling efficiency between the plasmonic and photonic waveguides is estimated by calculating vector overlap integral in the following form [6, 26]

$$\frac{|\iint_A \mathbf{E}_1 \times \mathbf{H}_2 \cdot \hat{\mathbf{z}} dxdy| \, |\iint_A \mathbf{E}_2 \times \mathbf{H}_1 \cdot \hat{\mathbf{z}} dxdy|}{|\iint_A \mathbf{E}_1 \times \mathbf{H}_1 \cdot \hat{\mathbf{z}} dxdy| \, |\iint_A \mathbf{E}_2 \times \mathbf{H}_2 \cdot \hat{\mathbf{z}} dxdy|} \tag{1}$$

#233873 - $15.00 USD Received 5 Feb 2015; revised 24 Mar 2015; accepted 24 Mar 2015; published 1 Apr 2015

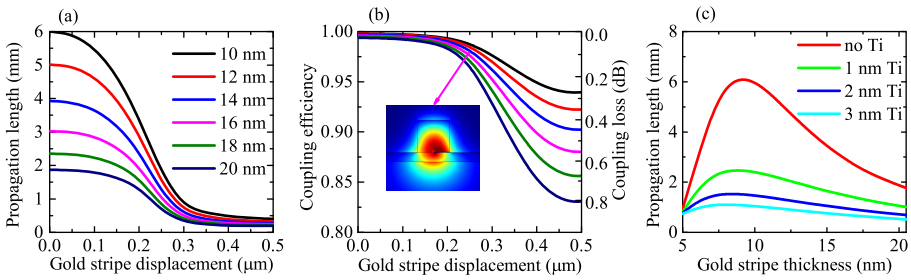

Fig. 2. Dependence of (a) propagation length and (b) coupling efficiency on gold stripe displacement for different gold stripe thicknesses of 10–20 nm. The curves in (b) share the same legend as in (a). Inset in (b) shows field distribution of $\mathbf{E}_y$ with the gold stripe displacement of 250 nm and gold thickness of 16 nm. (c) Influence of titanium intermediate layer on propagation length of LR-DLSPP mode as a function of gold stripe thickness.

where $\mathbf{E}_1$, $\mathbf{E}_2$, $\mathbf{H}_1$ and $\mathbf{H}_2$ are the electric fields and magnetic fields of the in-coupling and out-coupling modes. The waveguide maintains more than 97% coupling efficiency even when the gold stripe displacement is as large as 200 nm regardless of the gold stripe thickness [Fig. 2(b)]. This shows again good fabrication tolerance to the placement of the gold stripe.

In fabrication, it's a very common and necessary process to include a thin Ti layer beneath gold film to promote adhesion between gold and dielectric materials. However, accidentally, the introduction of this Ti layer can place huge influence on the performance of the structure. In our case, 3 nm thick of titanium ($\mathbf{t}_{Ti}$=3 nm) is deposited beneath the gold film. As shown in Fig. 2(c), this thin layer of titanium brings very large loss to the waveguide. Even when only 1 nm thick titanium film is used, in the case of $\mathbf{t}_{Au}$=15 nm, the propagation length drops about 2 times from 3.5 mm to 1.6 mm. If $\mathbf{t}_{Ti}$=3 nm, the propagation length decreases to 0.76 mm. Such strong influence of titanium layer on propagation losses is due to its high imaginary part of relative permittivity compared to gold, thus resulting in large absorption. It should be noted that it is only an estimation of titanium adhesion layer influence, since for such thicknesses and evaporation method of fabrication it is no longer a continuous homogenous layer but instead individual islands.

3. Experimental results

Phase- and amplitude-resolved near-field investigation of LR-DLSPP waveguides was conducted using scattering-type scanning near-field optical microscope (s-SNOM) from NeaSpec, based on atomic force microscope (AFM) that uses standard commercial platinum-coated Si tips as near-field probes (Arrow NCPt from NanoWorld). Our s-SNOM was operated in transmission mode, when the sample is illuminated from below (see the detailed setup layout in [27]). In order to excite the waveguiding mode from the cleaved edge (end-fire excitation), a small 45-degree mirror was attached to the sample holder in front of the waveguide entrance [Fig. 3(a)]. First, the optical configuration of the setup (position of the lower parabolic mirror) was adjusted with red probe beam ($\lambda \sim 630$ nm) [Fig. 3(b)]. In optimal adjustment a bright spot was observed at the input (cleaved edge) and output grating of the waveguide, indicating overlap of the focused spot with waveguide entrance and waveguiding in dielectric ridge at wavelength of 630 nm. Then the source was changed to telecom laser (λ = 1500 nm), and the sample was scanned in AFM tapping mode (AFM tip can be seen in Fig. 3(b), displaced from the waveguide), with a tapping amplitude of $\sim$ 50 nm. The near-field, scattered by the tip, was guided by top parabolic mirror towards detector, where it was overlapped with an interfering modulated reference beam (pseudoheterodyne detection [28]), providing complex-valued

#233873 - $15.00 USD Received 5 Feb 2015; revised 24 Mar 2015; accepted 24 Mar 2015; published 1 Apr 2015

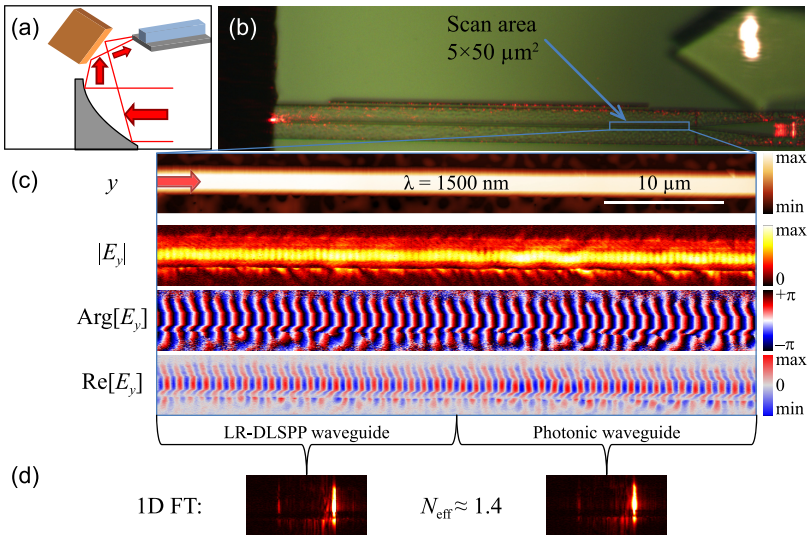

Fig. 3. (a) Schematic demonstration of the implementation of 45-degree mirror in transmission-mode s-SNOM setup. (b) Top view of the waveguide and shifted SNOM-probe under excitation with red probe beam. Off-side trench reflects the position of the gold stripe in the waveguide. (c) Pseudocolour s-SNOM images of topography and complex-valued near-field at = 1500 nm (represented in terms of amplitude, phase, and real part). The propagation direction of the mode is illustrated with arrow. (d) One-dimensional Fourier transformation of near-field map, used for evaluation of effective mode index and back reflection.

near-field (i.e., amplitude and phase of near-field). Due to a dominating dipole moment of a tip along its axis (i.e., along y-axis), the recorded s-SNOM images represents a distribution of the y-component of the electric field, $\mathbf{E}_y$ [29]. Since only the sample is moving during the scan in standard s-SNOMs, here we employed synchronous movement of the lower parabolic mirror together with the sample during the scan in order to keep the same alignment of waveguide excitation.

Experimental scan of the waveguide, containing both plasmonic and photonic section [Fig. 3(c)], revealed no observable change in the near-field amplitude upon transition, indicating low coupling losses between LR-DLSPP and photonic waveguide. The interface between plasmonic and photonic waveguides was identified by off-side trench [Fig. 3(b)], fabricated specifically to reflect the position of the gold stripe under the dielectric ridge. A one-dimensional Fourier transformation (1D FT) of the complex-valued near-field map allowed determination of the effective mode index for each waveguide, which appeared to be ~ 1.4, the same for plasmonic and photonic waveguides (within the accuracy of 0.05). Also it indicated a weak back reflection of the waveguiding mode (estimated to be $\sim 2\%$ in intensity) in both plasmonic and and photonic waveguides, which is probably a reflection from the output grating. Unfortunately, the propagation length of LR-DLSPP mode could not be measured due to relatively small scanning range (100 μm compared to the expected mm-long propagation length) and some fluctuations of the near-field (which can be ascribed to some imperfections in measured or fabricated topography of the waveguide). Overall, near-field experiments supported our initial statement, that the effective mode indices and modal field profiles in LR-DLSPP waveguide and the same waveguide without gold stripe are very similar, with little coupling loss between them.

The transmission from the waveguides is measured by our home-made experiment setup,

#233873 - $15.00 USD Received 5 Feb 2015; revised 24 Mar 2015; accepted 24 Mar 2015; published 1 Apr 2015

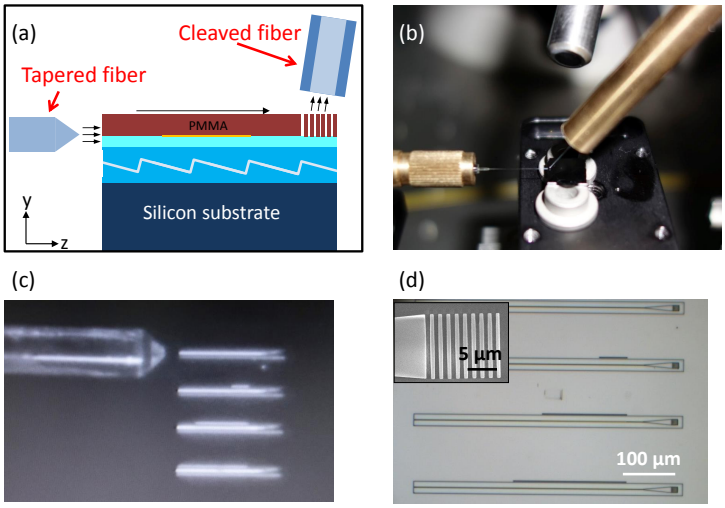

Fig. 4. (a) Schematic illustration and (b) photo of the experimental setup for measuring the transmission through the waveguides. (c) Top-view optical microscope image of the cleaved waveguides and the aligned tapered-lensed fiber. (d) Top-view optical microscope image of the uncleaved sample, including four waveguides with different lengths of embedded gold stripe, with grooves outside of the waveguides reflecting the length and position of gold stripes. Inset presents the scanning electron microscope image of the grating in the end of the waveguides.

which is schematically demonstrated in Fig. 4(a). Firstly, a broad-band linear-polarized near-infrared light is coupled into the cleaved end of the waveguide using a tapered-lensed polarization-maintaining single-mode fiber. After the light propagates through the photonic waveguide with plasmonic section, it is scattered off by a grating at the end of the waveguide and collected by a cleaved single-mode fiber [Fig. 4(b) and 4(c)]. The grating has 10 periods, with a period of 1.2 μm, and a duty cycle of 50% [see inset in Fig. 4(d)]. In order to measure both the propagation loss of LR-DLSPP mode and the coupling loss between photonic and plasmonic modes, we fabricate waveguides with four different lengths of gold stripe, which are 0, 50, 150 and 200 μm respectively, and grooves outside of the waveguides, reflecting the length and position of gold stripe [Fig. 4(d)].

In the experiment, we measured the transmission through the waveguides from four samples, every one of which has four waveguides with different lengths of gold stripe. Figure 5(a) shows the averaged transmission from the waveguides in the wavelength range of 1530–1630 nm, with the error bar showing the standard deviation. Here we assume that propagation losses in the photonic waveguide sections are negligible due to the short lengths. Then the transmission can be calculated as the following equation

$$T = C_{com}(C_{\mathrm{pl-ph}})^{n} \exp\left(-\frac{L_{stripe}}{L_{prop}}\right) \tag{2}$$

where T is transmission, C_{com} is common losses (at the entrance of waveguide, i.e., at the cleaved edge, and the exit, i.e., at the grating, and in the setup, i.e., through fibers), which we consider as a constant here, C_{pl-ph} is coupling losses at plasmonic-photonic interface, n is number of interfaces (2 for waveguides with plasmonic stripe and 0 for photonic waveguide),

#233873 - $15.00 USD Received 5 Feb 2015; revised 24 Mar 2015; accepted 24 Mar 2015; published 1 Apr 2015

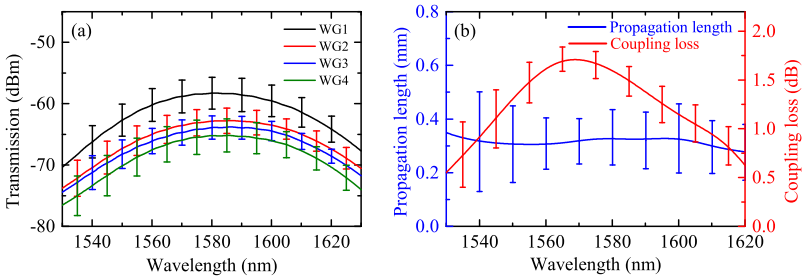

Fig. 5. (a) Measured transmission of the four waveguides after averaging all the results from four samples. WG1 is the waveguide without gold stripe. WG2, WG3 and WG4 stand for the waveguides with the gold stripe length of 50, 150 and 200 μm, respectively. (b) Propagation length and coupling loss as a function of the wavelength. Error bar in both figures shows the standard deviation.

L_{stripe} is length of the stripe and L_{prop} is propagation length. Therefore, for each free-space wavelength, there are 4 waveguides which means we have four different equations, based on which C_{pl-ph} and L_{prop} can be easily determined by fitting with least-square method [Fig. 5(b)]. The propagation length and coupling loss at 1550 nm is about 0.3 mm and 1.25 dB (or 75% coupling efficiency). The expected (from simulations) increase in the LR-DLSPPW mode propagation length with the increase of the wavelength (by $\sim$ 20%) is obscured in the experimental characterization due to a relatively large error of measurements [Fig. 5(b)], which is in turn related to a relatively small number of the fabricated waveguides of different lengths [Fig. 5(a)]. The measured propagation length is about half smaller than the theoretical prediction of 0.76 mm. The increased propagation loss could stem from the variation of $\mathbf{t}_{Ti}$ and $\mathbf{t}_{Au}$, which may be actually larger than 3 nm and 15 nm [Fig. 2(c)]. Besides, displacement of gold stripe and gold stripe roughness can also contribute to the loss. The increased coupling loss may also result from the same reasons. However, compared to other reports [4, 6] of measured coupling loss between plasmonic and photonic waveguides, ranging from 1 to 4.5 dB, our result (1.25 dB) is still pretty competitive, let alone the great improvement potential of about 0.05–0.2 dB according to the theoretical prediction [Fig. 2(b)].

4. Conclusion

In this paper, we have presented efficiently interfaced photonic and plasmonic waveguides by exploiting the LR-DLSPPW configuration. Due to their similar mode profiles, theoretical calculations predict extremely high coupling efficiencies (>97%) between the plasmonic and photonic waveguides at telecom wavelengths, even when significant gold stripe displacements are allowed. The measured coupling efficiency and propagation length at 1550 nm are on average close to 75% and 0.3 mm, respectively. Even though the experimentally obtained characteristics are worse than those predicted by simulations, both coupling loss and propagation length are still among the best characteristics demonstrated experimentally. Moreover, by decreasing the thickness of titanium and optimizing the fabricating process, the propagation length and coupling efficiency can be improved significantly. The results obtained demonstrate that LR-DLSPPWs can efficiently be interfaced with photonic (dielectric) waveguides, opening thereby new perspectives for realization of hybrid photonic-plasmonic components and circuits.

#233873 - $15.00 USD Received 5 Feb 2015; revised 24 Mar 2015; accepted 24 Mar 2015; published 1 Apr 2015

Acknowledgment

The authors would like to extend their gratitude to Valentyn S. Volkov, Alexander S. Roberts, Cesar E. Garcia-Ortiz, Anders Pors, Zhanghua Han and Ilya P. Radko for the help in this work. The authors also gratefully acknowledge financial support from the European Research Council, Grant 341054 (PLAQNAP).

#233873 - $15.00 USD Received 5 Feb 2015; revised 24 Mar 2015; accepted 24 Mar 2015; published 1 Apr 2015